Engineered Swift Equilibration of brownian particles: consequences of hydrodynamic coupling

S. Dago[1], B. Besga [1], R. Mothe[1], D. Guéry-Odelin[2], E. Trizac [3], A. Petrosyan[1], L. Bellon[1*], S. Ciliberto [1]

1 Univ Lyon, Ens de Lyon, Univ Claude Bernard Lyon 1, CNRS, Laboratoire de Physique, F-69342 Lyon, France
2 Laboratoire de Collisions Agrégats Réactivité, CNRS, UMR 5589, IRSAMC, France
3 Université Paris-Saclay, CNRS, LPTMS, 91405, Orsay, France.
* ludovic.bellon@ens-lyon.fr

May 12, 2020

Abstract

We present a detailed theoretical and experimental analysis of Engineered Swift Equilibration (ESE) protocols applied to two hydrodynamically coupled colloids in optical traps. The second particle slightly perturbs (10% at most) the response to an ESE compression applied to a single particle. This effect is quantitatively explained by a model of hydrodynamic coupling. We then design a coupled ESE protocol for the two particles, allowing the perfect control of one target particle while the second is enslaved to the first. The calibration errors and the limitations of the model are finally discussed in details.

Contents

arXiv:2005.04939v1 [cond-mat.stat-mech] 11 May 2020

1   Introduction

Speeding-up an equilibration process is a delicate task, because the relaxation time is an intrinsic property of a system which depends on parameters such as the dissipation, the potential strength, the inertia, or the number of degrees of freedom. Furthermore, when a control parameter is suddenly changed, the system may pass from states that widely differ from the target one. One way of speeding up a specific transformation between well defined equilibrium states is to apply complex protocols in which the time dependence of one or several control parameters is tuned in a highly specific fashion, to reach the final target in a selected short amount of time. This problem, related to optimal control theory, can be traced back to Boltzmann [1–3]. It has recently received sustained attention within the framework of the so-called "Shortcut To Adiabaticity" protocols, which study such complex procedures for specific transformations [4, 5].

We are interested here in overdamped systems in contact with a thermostat, for which we have defined protocols of Engineered Swift Equilibration (ESE) and applied them to the control of Brownian particles trapped by optical tweezers [6]. For example, one can perform the compression of a single particle trapped in an harmonic potential by increasing its stiffness K between an initial state in equilibrium at K_i and a final state in equilibrium at K_f. After a sudden change in K (STEP protocol) the bead will equilibrate with its natural relaxation time. Using an ESE protocol for the time evolution of $K(t)$, the same final state can be reached several order of magnitude faster than STEP [6]. We will refer to this fast compression protocol as the **basic ESE**. When designing these protocols, one of the key questions lies in the stability against external perturbations. In this context, we tackle in this article the case of two particles trapped in different potentials but hydro-dynamically coupled, to understand to what extent the equilibration dynamics imposed by the *basic ESE* is modified by the hydrodynamic interactions with another bead. A deep understanding of the physical consequences of the coupling on the particles behaviour (correlation) is necessary to work out the consequences of this perturbation. The goal here is twofold: on the one hand, it is a simple bench test to probe the robustness of the *basic ESE*. Indeed, we can see the second particle as a perturbation to the first, and monitor how far the protocol misses its target if we neglect this perturbation. And on the other hand, it is a first step towards the control of more complex systems with several degrees of freedom.

The article is organised as follows: in a first part, we investigate robustness of the *basic ESE* to the coupling interaction. To do so, we conduct experiments using the experimental set up described in section 2, and present the results in section 3. Then, in section 4, to support our experimental results, we use a simple model from [7–10] to describe the coupled system, and predict the dynamics of the correlations at equilibrium and of the moments in general. We then turn to the second goal of the paper: extend the scope of ESE protocols to more complex system. The model used is precise enough to be at the basis of the construction of new ESE protocols adapted to the coupled system. In particular we explore in section 5 the construction of ESE protocols that do not depend on the coupling intensity, and are thus very robust. We then demonstrate experimentally the validity of this extension. Finally we will draw the experimental limits of this new strategy in section 6.
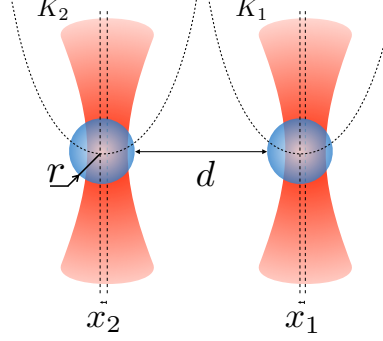
2 Experimental set up and method

Figure 1: Two Brownian particles trapped by optical tweezers into two harmonic potentials of stiffness K_1 and K_2. x_j represents the position of the particle $j = 1, 2$ relative to its trap center, and in the following, $\widetilde{x}_j = x_j + x_j^0$ represents the absolute position. d is the mean distance to contact between the two particles of radius $r = 1 \, \mu$m: $d = |x_2^0 - x_1^0| - 2r$.

To test the robustness of the *basic ESE* to the coupling interaction, we perform experiments on two close silica beads of radius $r = 1 \, \mu$m immersed in miliQ water (to avoid trapping impurities) at a temperature T and trapped by two optical tweezers separated by the distance d (see fig. 1). We use a very small concentration of silica micro-spheres in water and a specific design of the cell containing the particles, in order to have very few beads in the measuring volume. This allows us to take long measurements without any spurious perturbation. The two beads are trapped at $20 \, \mu$m from the bottom plate of the cell. The traps are realized using near-infrared single mode DPSS laser (Laser Quantum, $\lambda = 1064 \, $nm used at a power of $1 \, $W) expanded and injected through an oil-immersed objective (Leica, $63 \times$ NA 1.40) into the fluid chamber. Acousto-Optic Deflector (AOD) controls the intensity of the trapping beam and its positions with the amplitude and frequency of the control signal respectively. Thus we create two harmonic potentials at a distance d along the x direction $U_j(\widetilde{x}_j, t) = -K_j(t)(\widetilde{x}_j - x_j^0)^2/2$, with $j = 1, 2$, where $\widetilde{x}_j$ are the absolute particle positions. The potential minimum x_j^0 and stiffness K_j are respectively controlled by the AOD input signal frequency and amplitude. Furthermore, as the AOD responds linearly, a sum of sinus of different frequencies results in two potentials $U_{j=1,2}$ separated by a distance proportional to the difference between the sinuses frequencies. We can also use a second version of the setup with two AOD (one for each trap) to have two perfectly uncoupled static traps with orthogonally polarized beam (which is needed in particular when $K_1(t) \neq K_2(t)$). The detection of the particle position is performed using a fiber coupled single mode diode laser (Thorlabs, $\lambda = 635 \, $nm, power $1 \, $mW) giving around $100 \, \mu$W after the density filters, which is collimated after the fiber and passed through the trapping objective. The forward-scattered detection beam is collected by a condenser (Leica, NA 0.53), and its back focal-plane field distribution projected onto a four quadrant detector (QPD from First Sensor with a bandpass of $1 \, $MHz with custom made electronic) which gives a signal proportional to the particle position. Before every acquisition, a calibration procedure described in Appendix A.1 is conducted.

As regards the acquisition process of ESE responses, we have to follow a method that compares the situation when the particles are strongly coupled ($d \lesssim r$), with the situation when the coupling is negligible ($d \gg r$), in order to conclude on the perturbation induced by the coupling. Because the procedure is very sensitive to the instrument calibration and external parameters, to compare properly the 2 cases described above, we apply the following procedure: we start with a small distance and record the particle position during a dozen of ESE protocols, then we quietly separate the 2 particles and record again a dozen protocols, before bringing again the 2 particles closer and restart the cycle. Doing so enables us to compare the response to the ESE protocol in the coupled and uncoupled cases in the same experimental conditions. The recording lasts 10000 protocols to reduce statistical uncertainty. The same method can be adapted to any comparison purposes between two situations, the point being always to maintain the same working conditions between the two acquisitions.

3   Consequences of coupling perturbation on the *basic ESE protocol*

This section aims to see to what extent the response of the particle to the *basic ESE* deviates from the 0-coupling case successfully tested in ref. [6], when it is impacted by the coupling perturbation created by another particle at distance d.

Indeed, the *basic ESE* defined in ref. [6] is designed for a single particle trapped in the potential $U(t) = \frac{1}{2}K(t)x^2$, and whose over-damped dynamics is described by a Langevin Equation that introduces the friction coefficient $\gamma = 6\pi\eta r$, η being the kinetic viscosity and $r = 1\,\mu$m the radius of the particle. The *basic ESE* consists in changing the stiffness over a period of time t_f to reach a new equilibrium at K_f. The corresponding stiffness profile is the following, using the dimensionless quantities $k(t) = K(t)/K_i$ (in particular $k_f = K_f/K_i$), $s = t/t_f$ and $\Gamma = \gamma/(K_i t_f)$ (ratio of relevant timescales):

$$k(s) = 1 + (k_f - 1)(3 - 2s)s^2 - \frac{3\Gamma(k_f - 1)(s - 1)s}{1 + (k_f - 1)(3 - 2s)s^2}. \tag{1}$$

One may expect that if the ESE final time t_f is small enough compared to the characteristic correlation time τ_{corr}, the particles will behave as in the free case. To test this hypothesis we study the evolution of the variance of the first particle for what we call the **symmetric protocol**: stiffness of both wells is simultaneously driven ($K_1(s) = K_2(s) = K(s)$) according to the *basic ESE* in eq. (1). In the following we associate to the first particle variance $\langle x_1^2 \rangle$ the dimensionless quantity $\sigma_{11} = K_i \langle x_1^2 \rangle/(2k_B T)$. In the *symmetric protocol* context $\sigma_{11} = \sigma_{22} = \sigma$. We apply this procedure for an ESE time t_f one order of magnitude smaller than the typical characteristic times $\tau_{\mathrm{corr}} \sim \tau_{\mathrm{relax}} \sim 15\,$ms. To cycle the procedure we use the stiffness profile of fig. 2 (left) for both traps: a simple step decompression followed by the *basic ESE*. The experimental results are plotted in plain lines on fig. 2 (right) for small distance in purple and large distance in black. In response to the step decompression, the particle reaches equilibrium in its natural relaxation time τ_{relax}. We notice that the coupling also affects this natural relaxation (by slightly slowing it down). Then we apply *basic ESE protocol* to both wells for compression, and we observe that at small d the coupling induces a rebound in the variance evolution (indicated by the red arrow on the figure) and prevents the particle to reach equilibrium in the expected time. The ESE is also very sensitive to other external
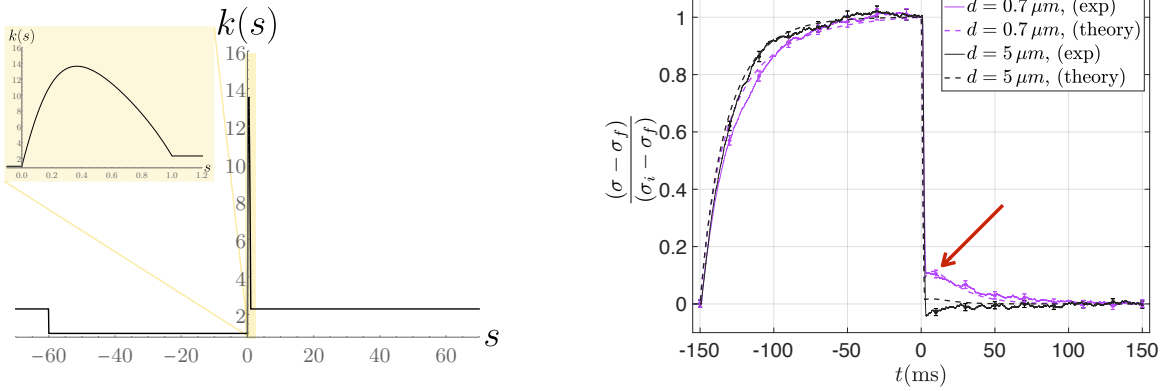
Figure 2: (Left) The stiffness profile applied to both wells: a step decompression at $s = -60$ followed by a *basic ESE* protocol for compression for $0 < s < 1$. This procedure is called the *symmetric protocol*. At $t = -150\,\mathrm{ms}$ (or equivalently $s = -60$), the stiffness jumps from K_f to $K_i = 4 \times 10^{-7}\,\mathrm{N/m}$ such as $K_f/K_i = 2.3$. At $t = 0$ the particle is thus in its initial equilibrium when we apply an ESE protocol finishing at t_f (i.e. $s = 1$) to bring back the particle to its final state at K_f. The ESE parameters are: $t_f = 2.5\,\mathrm{ms}$, $K_i = 4 \times 10^{-7}\,\mathrm{N/m}$, $k_f = 2.3$, and $\Gamma = 18.9$. This stiffness profile emphasizes the difference between the relaxation after a step function, and the response to the ESE protocol. (Right) Normalized variance of the first particle $(\sigma(t) - \sigma_f)/(\sigma_i - \sigma_f)$ corresponding to the *symmetric protocol*. The plain lines are the experimental results with their error bars each 200 points. The dashed curves are numerically computed from the theoretical analysis of section 4, plugging the experimental parameters from the calibration. The same process is applied for particles separated by $d = 5\,\mu\mathrm{m}$ (black) and $d = 0.7\,\mu\mathrm{m}$ (purple) corresponding respectively to coupling constant (introduced in section 4) $\epsilon = 0.21$ and $\epsilon = 0.5$. A small rebound highlighted by the red arrow (around 10% of the step) and long relaxation time are visible for close particles.

perturbations, indeed a small drift in calibration may be responsible for the very small slip of the black curve under its final value at t_f. These observations are very reproducible and one may see in Appendix A.2 complementary results highlighting the increase of the rebound height with the intensity of the coupling.

To put it in a nutshell, fig. 2 highlights that even though the protocol is designed to be much faster than the coupling characteristic time, the coupling perturbation impacts the response to the *basic ESE*. Our sensitive experimental setup enables us to observe experimentally the tiny effect of hydrodynamic coupling: the particle variance observes a rebound at t_f and will not reach equilibrium before its natural relaxation time. Nevertheless *basic ESE* is rather robust as for moderate coupling, this bounce is modest compared to the natural relaxation amplitude evolution. Indeed *basic ESE* still provides correct results, with a 10% deviation to the 0-coupling case. This means that a measure with a poor statistics will hide the effect inside the statistical error.

It remains to be seen whether this experimental results can be supported by a theoretical analysis. That is why we will devote the next section to study the coupled system's dynamics, first in equilibrium and then when driven by the *symmetric protocol*.

4 Theoretical analysis

To describe the evolution of two trapped brownian particles hydrodynamically coupled, we use coupled Langevin equations,

$$\begin{pmatrix} \dot{x}_1 \\ \dot{x}_2 \end{pmatrix} = \mathcal{H} \begin{pmatrix} F_1 \\ F_2 \end{pmatrix}, \tag{2}$$

where x_j is the position of the particle $j = 1, 2$ relative to its trapping position (see fig. 1), $\dot{x}_j$ is the time derivative of x_j, and $\mathcal{H}$ is the hydrodynamic coupling tensor. The Langevin equations govern the system evolution in general whether or not it is at equilibrium. Besides, the Langevin equations (2) includes no acceleration term: we assumed the over-damped regime which is fully justified for colloidal objects (see Appendix A.3). At equilibrium the forces acting on the particles are:

$$F_j = -K_j x_j + f_j, \tag{3}$$

where K_j is the stiffness of the trap j and f_j is the Brownian random noise. For two identical particles of radius r separated by a distance d (see fig. 1), assuming that their displacements are small compared to the mean distance between them, the hydrodynamic coupling tensor reads [7–10]:

$$\mathcal{H} = \frac{1}{\gamma} \begin{pmatrix} 1 & \epsilon \\ \epsilon & 1 \end{pmatrix}. \tag{4}$$

In some approximations described in Appendix A.4 we can write $\epsilon = \frac{3}{2}\nu - \nu^3$, where $\nu = r/(2r + d)$.

Let us first study how the particles behave at equilibrium (K_j constant in time), and in particular how they influence their neighbour. At equilibrium the two particles are statistically independent: $\langle x_1 x_2 \rangle_{eq} = 0$, $\langle x_1^2 \rangle_{eq} = k_B T / K_1$, and $\langle x_2^2 \rangle_{eq} = k_B T / K_2$ (with k_B the Boltzmann's constant and T the bath temperature). However, the 2 particles are coupled in time by eq. (2). Extending the work of refs. [9, 11] to the more general case of two potentials of different stiffnesses, we show in Appendix A.5 that the equilibrium auto-correlations $\langle x_j(0)x_j(t) \rangle$ and cross-correlations $\langle x_j(0)x_k(t) \rangle$ (with $j \neq k$) of positions read as:

$$\langle x_1(t)x_1(0) \rangle = \frac{k_B T}{2 K_1 \kappa} \left[e^{-\frac{t}{\tau_+}} (K_1 - K_2 + \kappa) + e^{-\frac{t}{\tau_-}} (K_2 - K_1 + \kappa) \right], \tag{5}$$

$$\langle x_2(t)x_2(0) \rangle = \frac{k_B T}{2 K_2 \kappa} \left[e^{-\frac{t}{\tau_+}} (K_2 - K_1 + \kappa) + e^{-\frac{t}{\tau_-}} (K_1 - K_2 + \kappa) \right], \tag{6}$$

$$\langle x_1(t)x_2(0) \rangle = \frac{\epsilon k_B T}{\kappa} \left[e^{-\frac{t}{\tau_+}} - e^{-\frac{t}{\tau_-}} \right], \tag{7}$$

with

$$\kappa = \sqrt{(K_1 - K_2)^2 + 4\epsilon^2 K_1 K_2}, \tag{8}$$

$$\tau_- = \frac{2\gamma}{K_1 + K_2 - \kappa}, \tag{9}$$

$$\tau_+ = \frac{2\gamma}{K_1 + K_2 + \kappa}. \tag{10}$$

We report the computed behaviour in fig. 3. Those correlation functions involve two characteristic times τ_+ and τ_- that are very close to the natural relaxation time of the harmonic
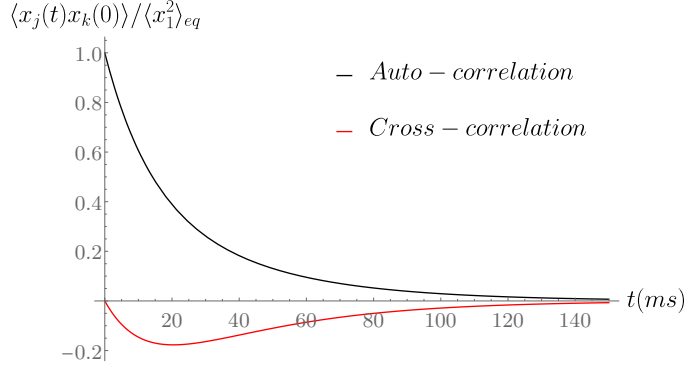
Figure 3: Auto and cross-correlation functions normalized by $\langle x_1^2 \rangle_{eq}$ as a function of time, when $\gamma = 1.88 \times 10^{-8}$ sN/m, $K_1 = K_2 = 10^{-6}$ N/m and $d = 1\,\mu$m, so that $\sigma_{11,eq} = k_B T / K_1 = 4 \times 10^3$ nm^2 and $\epsilon = 0.46$. We recover at $t = 0$ the values of the moments at equilibrium, in particular $\sigma_{12,eq} = 0$.

well $\tau_{\text{relax}} = \gamma/K_1 \sim 15\,$ms. We consequently introduce a slow mode and a fast mode associated respectively to τ_- and τ_+. The slow mode vanishes when $x_1 \propto x_2$, and the fast mode when $x_1 \propto -x_2$: ie correlation enhances the fast mode (correlated mode) and anti-correlation the slow mode (anti-correlated mode). In the symmetric case, the two modes may be interpreted as the barycentre of the system $x_M = (x_1 + x_2)/2$, and the fictitious particle $x_\mu = (x_2 - x_1)/2$. Naturally, x_μ embodies the slow mode and x_M the fast one, as the evolution of x_μ demands a fluid displacement between the particles, meanwhile the barycentre evolution relies on the fact that one sphere tends to drag the other in its wake (details in [9]). As far as auto-correlation functions are concerned, the shape of decaying exponential in fig. 3 is rather common. The negative cross correlation might be surprising at first. This feature stems from the fact that the cross correlation has to vanish at $t = 0$ (a consequence of independence at equilibrium), supplemented by the longer lived nature of the anti-correlated mode (associated to x_μ) as compared to the correlated mode (associated to x_M).

We now focus on the dynamics of the particles when the potentials change with time. It proves convenient to convert the coupled Langevin equations into equations describing the dynamics of the moments $\langle x_1^2 \rangle(t)$, $\langle x_2^2 \rangle(t)$ and $\langle x_1 x_2 \rangle(t)$. Using the dimensionless quantities $\sigma_{jk} = K_{1,i}\langle x_j x_k \rangle/(2k_B T)$, we obtain the following system to describe the evolution of the moments (see Appendix A.6):

$$\Gamma \frac{d\sigma_{11}}{ds} = -2k_1\sigma_{11} - 2\epsilon k_2\sigma_{12} + 1, \tag{11}$$

$$\Gamma \frac{d\sigma_{22}}{ds} = -2k_2\sigma_{22} - 2\epsilon k_1\sigma_{12} + 1, \tag{12}$$

$$\Gamma \frac{d\sigma_{12}}{ds} = -(k_1 + k_2)\sigma_{12} - \epsilon(k_2\sigma_{22} + k_1\sigma_{11} - 1), \tag{13}$$

where $s = t/t_f$ as before, $k_j(s) = K_j(s)/K_{1,i}$ ($K_{1,i}$ being the initial stiffness of the first well), and $\Gamma = \gamma/(K_{1,i}t_f)$. The above equations contain all the information on the dynamic of the system, as the joint probability distribution remains Gaussian out of equilibrium (see Appendix A.7) and is thus fully described by σ_{11}, σ_{22} and σ_{12}. The *basic ESE* in eq. (1) is defined in ref. [6] using eq. (11) without the cross term $\epsilon\sigma_{12}$ term. It thus cannot be operational

for the coupled system. Indeed we numerically compute the evolution of the variance of the first particle for the *symmetric protocol* where the stiffness of both wells is simultaneously driven according to the *basic ESE*. The results of these computations are summarized in fig. 4: it should be recalled that in the *symmetric protocol* context ($K_1 = K_2 = K$), the above equations simplify and $\sigma_{11} = \sigma_{22}$ can be written σ.
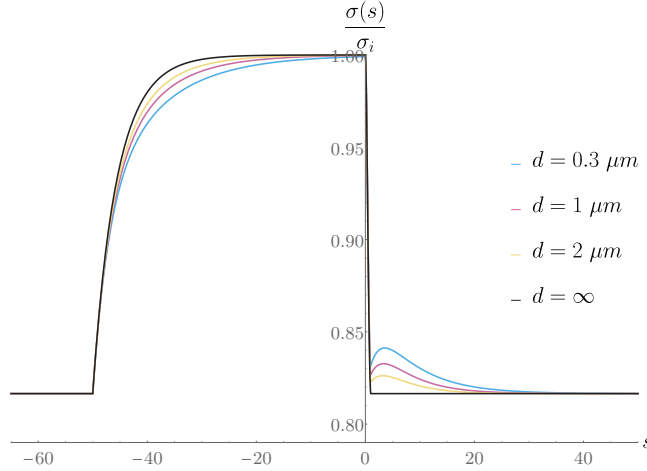

Figure 4: Evolution of the normalized variance of one particle in response to the *symmetric protocol* for different values of the distance d between the particles. The parameters of the ESE protocol (shaped as in fig. 2) are the following: $t_f = 2$ ms, $k_f = K_f/K_i = 1.5$, $K_i = 10^{-6}$ N/m, and $\Gamma = 9.42$. Without coupling (when $d = \infty$) the response to the ESE is shortcut to t_f. Meanwhile the hydrodynamic coupling results in a rebound on the variance curve, which no longer reaches its equilibrium value at t_f, but after a few natural relaxation times $\tau_{\text{relax}} \approx 15$ ms. As we would have expected from experimental results, the smaller the distance d, the higher the rebound and so the deviation from the 0-coupling case.

The theoretical predictions of fig. 4 seem to be in agreement with the experimental conclusions drawn in section 3. To confirm that the model prediction and the experimental curves match, we superpose in dashed lines on fig. 2 the theoretical curves obtained using the same ESE parameters and the external parameters from calibration. We see that the results are in very good agreement. Besides the validity of the theory during the preparation of the system at K_i confirms the good estimation of the external parameters by the calibration during the experiment.

The model of the hydrodynamic coupling proves to be precise enough to be used for ESE computations. We are thus equipped to propose a new strategy to drive a coupled system without any compromise on the shortcut efficiency. Indeed we can take into account the hydrodynamic coupling in the construction of a new ESE protocol thereby eliminating the small although spurious bounce identified above.
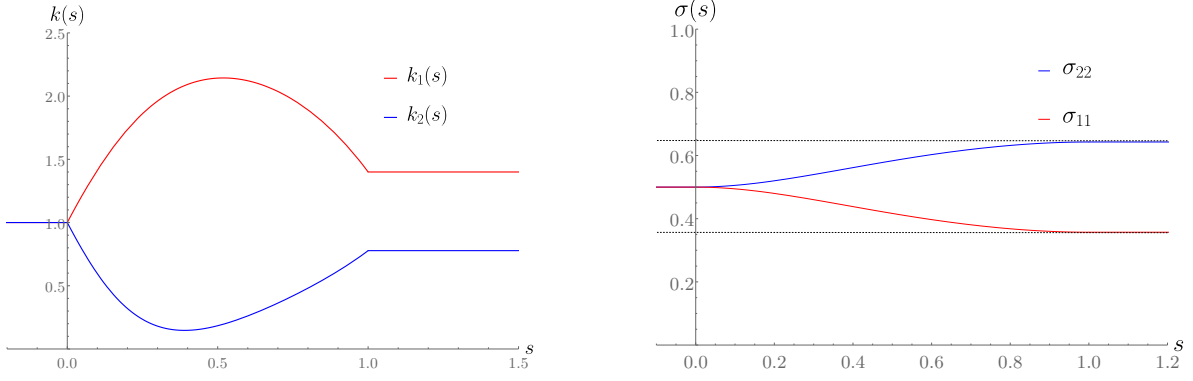
Figure 5: (Left) Profiles $k_1(s)$ and $k_2(s)$ computed for the *coupled ESE protocol* that maintains independence between the particles for parameters: $k_f = 1.4$, $K_i = K_{2,i} = 1.8 \times 10^{-6}\,\mathrm{N/m}$, $t_f = 2.5\,\mathrm{ms}$, and $\Gamma = 4.19$. While k_1 (red) reaches the target value at $s = 1$, the second well stiffness k_2 (blue) has to adapt itself. In particular its final stiffness value is determined by the other parameters of the ESE: $k_{2f} = k_{2i}k_f/(k_{2i}k_f + k_f - k_{2i})$. This protocol does not depend on the coupling constant ϵ and so works for any distance d between the particles. (Right) Result of the computation for the dimensionless variances of the two particles using the ESE protocol on top: σ_{11} in red, and σ_{22} in blue. The plot confirms that Boltzmann equilibrium (horizontal grey lines) is reached for both particles at initial and final times. Let us remind that $\sigma_{12} = 0$ all along.

5 Coupled ESE protocol

Our strategy to design a *coupled protocol* is now to look for an ESE scheme that would drive the first particle from $(t_i = 0, K_i)$ to (t_f, K_f) while being robust to coupling interaction. A solution to achieve this requirement is to design a protocol that does not depend on the coupling intensity (ie independent of the ϵ parameter). This strong constraint can be met if we demand particle independence at all time, that is to say $\langle x_1 x_2 \rangle(t) = 0$ during all the process and not only at equilibrium states. Indeed insofar as we require independence, the results no longer depend on the strength of the coupling.

As detailed in Appendix A.8, the independency requirement ($\sigma_{12} = 0$ during the process) enables us to simplify the evolution equations eq. (11)-(13) and to find an ESE protocol that meets the requirements detailed above: we find a shape for $k_1(s)$ and $k_2(s)$ independent of ϵ that satisfies the equilibrium at t_f of both particles (see fig. 5). The expression of $k_1(s)$ is therefore the same as the single particle case, but the second potential has to be driven appropriately with a different stiffness profile $k_2(s)$.

The price to pay to drive the particle 1 from $K_{1,i}$ to $K_{1,f}$ is to impose a nearly opposite profile on the second potential. In particular the final value of the second well stiffness $K_{2,f}$ is imposed by the parameters chosen for the first particle and is therefore not chosen a priori. Besides, a sum rule ensues, such that $k_1\sigma_{11} + k_2\sigma_{22}$ is conserved. This trend of the two wells to evolve in opposition in order to maintain independence can be explained by the correlation due to the coupling. Indeed we can interpret the coupling term ϵF_1 in eq. (2) as an extra random noise:

$$\gamma \dot{x}_2 = -K_2 x_2 + f_2 + \epsilon F_1. \tag{14}$$

This coupling term behaves as the random noises with the following characteristics (at equilibrium),

$$\langle \epsilon F_1 \rangle = -\epsilon K_1 \langle x_1 \rangle + \epsilon \langle f_1 \rangle = 0, \tag{15}$$

$$\langle \epsilon^2 F_1^2 \rangle = \epsilon^2 k_1^2 \langle x_1^2 \rangle + \epsilon^2 \langle f_1^2 \rangle = \epsilon^2 k_B T k_1 + \epsilon^2 \langle f_1^2 \rangle. \tag{16}$$

Thus if k_1 increases, the noise imposed to particle 2 by the coupling increases as well, and consequently so does the variance of particle 2. To pretend that the two particles are independent and that this augmentation of the variance of particle 2 is not due to the behaviour of the particle 1, the second well should open up. That is why to maintain a vanishing cross term $\sigma_{12} = 0$ the second well should behave in opposition to the first one (see fig. 5).

The experimental realisation of the *coupled protocol* is illustrated in fig. 6. We work with a distance $d = 0.8\,\mu$m between the particles to ensure strong coupling. We compare the response of the system when the two potentials are driven together with the *symmetric protocol*, with the response when we apply the *coupled ESE*.
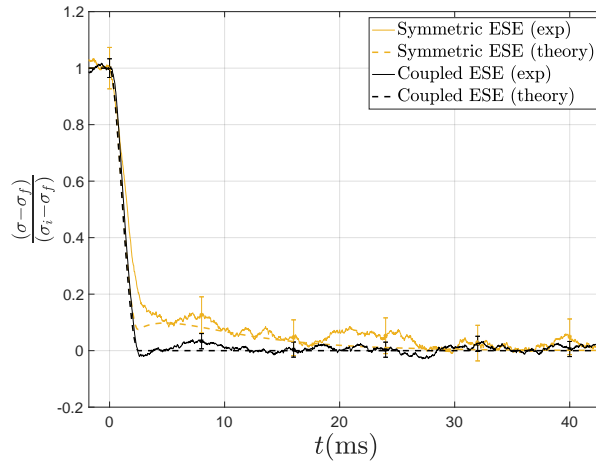

Figure 6: Normalized variance of the first particle when the potentials are driven by the *symmetric protocol* (yellow) or by the *coupled ESE protocol* (black). The parameters of the experiment are: $k_f = 1.4$, $K_{1,i} = K_{2,i} = 1.8 \times 10^{-6}\,$N/m, $t_f = 2.5\,$ms, $d = 0.8\,\mu$m, and thus $\epsilon = 0.49$ and $\Gamma = 4.19$. The *symmetric protocol* leads to the rebound predicted in section 4. On the contrary the *coupled protocol* designed to cancel the correlations between the particles works as expected: the rebound is essentially suppressed and the particle reaches equilibrium at t_f. Besides the experimental results (plain lines) are again in very good agreement with the theoretical predictions (dashed lines) using only measured parameters and no adjustable ones.

In this new set of experiments, the rebound in response to the *symmetric protocol* is naturally still present, but disappears when applying the *coupled ESE protocol*. This result validates the efficiency of enforcing independence for coupled particles. Indeed this protocol is very stable against the coupling interaction because it does not depend on the strength of the coupling (ϵ in our model). Thanks to this process we achieve the same efficiency of the shortcut to equilibrium we had on a single particle, but now for coupled ones. This

extension of the validity of ESE protocol has nevertheless a cost: the second particle, coupled to the particle of interest, has to be driven to a final state of equilibrium defined by the other parameters of the protocol (K_{2i} and k_f).
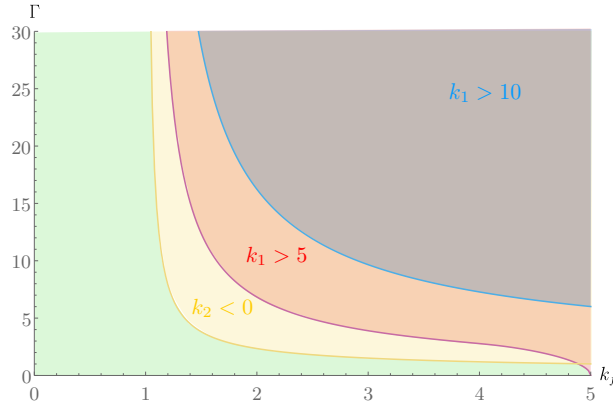
6 Limits and other approaches

Figure 7: Experimental limits of the *coupled ESE protocol* in terms of the speed-up parameter Γ. The yellow line represents the higher limit Γ should not exceed to maintain $k_2 > 0$, the red one to maintain $k_1 < 5$ and the blue one to maintain $k_1 < 10$. The requirement $k_2 > 0$ being the most restrictive, the limit to enforce in experiments is the yellow line that corresponds to $\Gamma_{lim,1}$. Thus, the working region where all the constraints are met is the green region. The yellow, red and blue regions delineate the domains where the various requirements are not true anymore.

We are experimentally facing two limitations on the realization of the *Coupled ESE*. First stiffnesses must remain positive (ie attractive potentials) and second they cannot exceed maximum values above which the particles can be damaged. Actually it is possible to mimic repulsive potentials and go beyond the first constraint [12], but with a basic optical tweezers set up, it is far more convenient to stick to positive stiffness. In the case of the *Coupled ESE* assuming that $k_{2,i} = 1$ and $k_f > 1$ this limitations reformulates as $k_2 > 0$ and $k_1 < k_{\max}$.

Using the expression of $k_2(s)$ and $k_1(s)$ we explicit the first limit as a constraint on the acceleration factor Γ, or equivalently on t_f and K_i as $\Gamma = \gamma/(K_i t_f)$. Indeed maintaining $k_2 > 0$ requires

$$\Gamma < \Gamma_{\lim,1} = \min[-\frac{1}{\dot{\sigma}_{11}(s)}, 0 < s < 1], \qquad (17)$$

$\Gamma_{\lim,1}$ depends on k_f (yellow curve in fig. 7): the more one wants to compress the well, the smaller Γ should be, and so the higher the t_f.

Concerning the second limit $k_1 < k_{\max}$ a similar computation gives us the corresponding constraint on Γ. We introduce:

$$\Gamma_{\lim}(s) = \frac{((k_f - 1)s^2(2s - 3) - 1)(k_{max} - 1 + (k_f - 1)s^2(2s - 3))}{3(k_f - 1)s(s - 1)}. \tag{18}$$

Then,

$$\Gamma_{\lim,2} = \min[\Gamma_{\lim}(s), 0 < s < 1]. \tag{19}$$

To summarize, we plot in the fig. 7 the maximum boundary $\Gamma_{\lim}$ to comply the constraints $k_2 > 0$ (yellow curve) and $k_1 < k_{\max}$ for $k_{\max} = 5$ (red curve) and $k_{\max} = 10$ (blue curve). As we expected the stronger the compression, the smaller is the region accessible for Γ that must remain under $\Gamma_{\lim}$. The limit $k_2 > 0$ is the most restrictive so that $\Gamma_{\lim,1}$ in yellow delimits the working region. To provide shortcuts outside the accessible region, some new strategies should be developed such as what has been done in ref. [13] for the *basic ESE*.

The *coupled ESE protocol* enforcing independence is a successful strategy to extend the family of ESE protocols to more complex systems that the *basic ESE* cannot drive with full efficiency. In the limits we highlighted above, this particular solution independent of ϵ turns out to be very powerful. Yet, the solution panel to the coupled case problem is wide, there is more to find in this direction. In particular, it is possible to guide the two particles in a symmetric and with an priori chosen target state with the same stiffness profile. This *symmetric coupled ESE protocol* detailed in Appendix A.9 has nevertheless a cost: cross-correlations appear during the process and vanish only at equilibrium. Without the independency requirement this protocol depends on the coupling intensity. That's why this ϵ dependent protocol is harder to implement experimentally. Further work is required to extend ESE protocols to more complex systems, and every solutions will have specific advantages and limits.

7 Conclusion

In conclusion, we explored shortcut to adiabadicity schemes for coupled systems: in particular two hydro-dynamically coupled particles. The first objective of this paper was to test the stability of the *basic ESE protocol* designed for single systems against the coupling interaction. Our experiments, in very good agreement with the model, proved its relative robustness: the coupling perturbation deviates the response of a dozen of percents from the 0-coupling case. It is nevertheless possible to work out explicitly ESE solutions that take due account of the coupling, and are therefore immune to it: this is the second message of the paper. The model used to describe the coupling proved reliable enough to build a new family of ESE solutions with the same method of retro-computing used to find the single particle ESE protocol. We thus propose a very robust protocol, because ϵ independent, that enforces independence between the particles. Experimental tests confirm the efficiency of this shortcut strategy within the experimental limits described in the last part of the paper. Other solutions can be investigated such as a symmetric protocol designed for coupled particles (more difficult to implement because ϵ dependent).

Acknowledgements

A   Appendix

A.1   Calibration procedure

As the effect under scrutiny is tiny, a very accurate calibration is necessary to observe it. Thus we detail in this section the calibration procedure conducted before the experimental tests of ESE protocols. It is performed as follows: first we have to find the correspondence between the amplitude A of the sine wave driving the AOD and the stiffness K applied by the optical trap to the particle. To do so, we acquire the position variance ($\sigma^2 = k_B T/K$) for different amplitudes A. This calibration curve enables us to convert the ESE protocol in driving amplitude for the AOD. Then, the only dependence on external parameters of the ESE protocol lies in the parameter $\Gamma = \gamma/(K_i t_f)$. To estimate Γ we conduct the acquisition of the cut off frequency [14] ($f_0 = K/(2\pi\gamma)$) when the particle is in the initial state of the ESE, $f_{0,i}$, through the Brownian noise spectrum in position of the particle for the initial value of amplitude A_i. Then we deduce $\Gamma = 1/(2\pi f_{0,i} t_f)$.

One may now wonder to what extent small drifts in calibration may impact the experimental results. Indeed during the typical time of our experiments (up to a few hours), we observe that the stiffness K and the parameter Γ decrease by a small amount: 4% at most. The stiffness variation can be a consequence of the variation of the AOD efficiency because the AOD warms up with time. On the other side, Γ is modified because of the following phenomena: the stiffness variation, the water viscosity dependency on the temperature, and the damping coefficient correction due to the distance h to the cell walls. Indeed at first order in r/h we can expand [15] $\gamma(T, h) = 6\pi r \eta_0(T) \times (1 + 9/16 \times r/h)$, with $\eta_0(T)$ decreasing of 2% per Kelvin, and the term in r/h leading to an additional 1% per $5\,\mu$m in h.

Those variation in K and Γ are thus small, leading to a small error on the ESE protocols themselves. Moreover, our cycle procedure of acquisition makes the comparison of protocols in equivalent experimental conditions. Drifts in Γ have the same consequences on the different responses we compare: the relative differences between the curves are only weakly sensitive to variations in Γ. Finally, drifts in K_i, K_f (thus σ_i, σ_f) are wiped out by plotting the normalised variance.

Besides, the local drift of the bath temperature due to the lasers power (measuring laser and trapping laser), amplifies the deviation of the particle variance also affected by the stiffness drift. Indeed the standard deviation σ can increase up to 2% during an acquisition. As we are studying σ jumps of 20% with ESE, it is better to get rid of the 2% error due to external parameters small deviations. To do so, we normalize the results at regular time intervals to minimize the drift effect in the results.

A.2   Complementary experimental results

As a complement to the results presented in fig. 2, we propose another experimental result in fig. 8. All the parameters are the same as in fig. 2 but the experiment is performed with 3 different distances between the particles. From it, we can affirm that first the results are very reproducible and always in very good agreement with the theory, and second that the
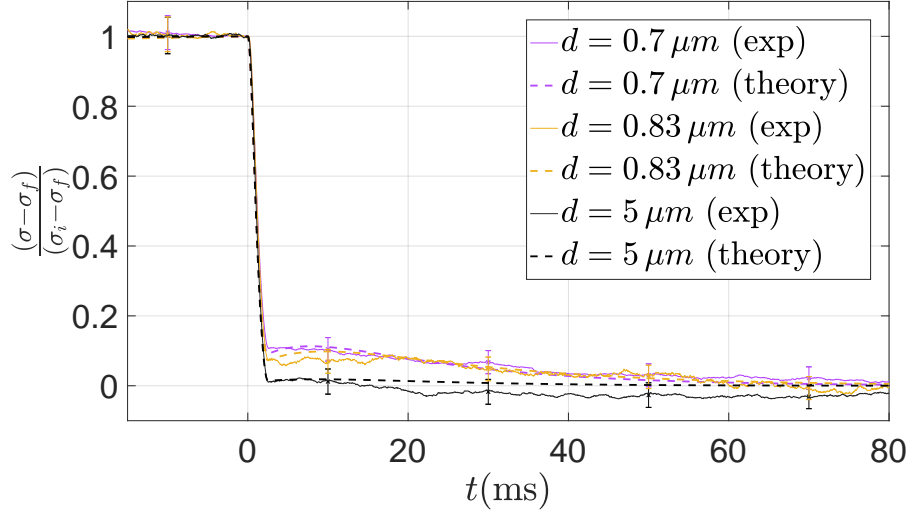
Figure 8: Same as fig. 2 but with three distances: $d = 5\,\mu$m in black, $d = 0.83\,\mu$m in yellow and $d = 0.7\,\mu$m in purple.

rebound decreases with the coupling as pointed at in fig. 4.

A.3 Over-damped regime

The influence of the inertia lasts on a characteristic time $\tau_{\text{inertia}} = m/\gamma = 2\mu r^2/(9\eta)$, with μ being the volumic mass of the particles. As we consider usual fluid like water, $\eta = 10^{-3}\,$Pa s, and $\mu = 10^3\,$kg m^{-3}. The point is then to compare τ_{inertia} to the time needed for the particle to diffuse on a distance equivalent to its diameter, τ_{diff}. In a usual diffusion process we have, $\tau_{\text{diff}} = (2r)^2/D$ using the diffusion coefficient $D = k_B T/(6\pi\eta r)$. Therefore, on the one hand, the r region where $\tau_{\text{inertia}} \ll \tau_{\text{diff}}$ corresponds to $r \gg 0.01\,$pm, this criterion is thus always met.

On the other hand, to get an upper limit on r, we compare τ_{inertia} to the characteristic time of the experiment $\tau_{ESE} = 1\,$ms. Indeed in the context of shortcut, the time of the ESE is more restrictive than the natural relaxation time $\tau_{\text{relax}} = \gamma/K \sim 15\,$ms. The assumption $\tau_{\text{inertia}} \ll \tau_{ESE}$ remains valid while $r \ll 70\,\mu$m. To conclude, the r region of the over-damped regime is $0.01\,$pm $\ll r \ll 70\,\mu$m.

We are thus working in the r region where the inertia faded too fast compared to the other phenomena to be noticed (indeed for $r = 1\,\mu$m, $\tau_{\text{inertia}} \sim 0.2\,\mu$s and $\tau_{\text{diff}} \sim 20\,$s): the regime is over-damped.

A.4 Model for Hydrodynamic coupling

The hydrodynamic interactions of the particles with the surrounding fluid are described with by their mobility matrix $\mathcal{H}$ (eq. (4)), which is also known as the Rotne-Prager diffusion tensor [7–9]. The Rotne-Prager diffusion tensor consists in adding third order correction in $(r/d)^3$ to the off-diagonal elements of the Oseen tensor. Under our experimental conditions, this corrections is always smaller than 3.5%. The form of the coupling ϵ depends on different

approximations. Here we assume ϵ to be constant: it involves only the distance between the wells d and not $(x_1 - x_2)(t)$. This assumption is supported by the following order of magnitudes: one particle can diffuse to its rms displacement $\delta x_{\mathrm{rms}} = \sqrt{k_B T/k} \sim 60\,\mathrm{nm} \ll d$. So that in first approximation $|x_1 - x_2| = d$ and $\epsilon = f(d)$. The expression of $\epsilon = f(d)$ is given by the Rotne-Prager approximation: for particle distances larger than $d = r$, $\epsilon = \frac{3}{2}\nu - \nu^3$, where $\nu = \frac{r}{d}$. The term ν becomes more important when particles are close to each other. At very short distances, when $d \lesssim r/10$, lubrication forces would have to be taken into account explicitly. On the contrary, in the small ν limit, we reach the Oseen approximation where $\epsilon = \frac{3}{2}\nu$.

A.5 Auto and Cross-Correlation

We start from the coupled Langevin equations (2):

$$\gamma \dot{x}_1 = -K_1 x_1 - \epsilon K_2 x_2 + f_1 + \epsilon f_2, \tag{20}$$
$$\gamma \dot{x}_2 = -K_2 x_2 - \epsilon K_1 x_1 + f_2 + \epsilon f_1, \tag{21}$$

and we use the Laplace Transform:

$$\widehat{x}(s) = \int_0^{+\infty} x(t) e^{-st} dt. \tag{22}$$

After having Laplace transformed the system (20), (21) we obtain (to simplify we stop indicating variables s and t: $\widehat{x}$ transformed functions implies s variable, and x functions t):

$$\gamma(s\widehat{x_1} - x_1(0)) = -k_1\widehat{x_1} - \epsilon k_2\widehat{x_2} + \widehat{f_1} + \epsilon\widehat{f_2}, \tag{23}$$
$$\gamma(s\widehat{x_2} - x_2(0)) = -k_2\widehat{x_2} - \epsilon k_1\widehat{x_1} + \widehat{f_2} + \epsilon\widehat{f_1}. \tag{24}$$

We then multiply the two above equations by $x_2(0)$ and take the mean value:

$$\gamma(s\langle\widehat{x_1}x_2(0)\rangle - \sigma_{12}^2) = -k_1\langle\widehat{x_1}x_2(0)\rangle - \epsilon k_2\langle\widehat{x_2}x_2(0)\rangle,$$
$$\gamma(s\langle\widehat{x_2}x_2(0)\rangle - \sigma_{22}^2) = -k_2\langle\widehat{x_2}x_2(0)\rangle - \epsilon k_1\langle\widehat{x_1}x_2(0)\rangle.$$

This system is then easy to solve (knowing the values of σ_{22} and σ_{12} at equilibrium at $t = 0$). The last step only consists in taking the Inverse Laplace Transform of the expressions obtained, leading to the expression of $\langle x_1(t)x_2(0)\rangle$ and $\langle x_2(t)x_2(0)\rangle$ of eqs. (7) and (6). We can reproduce the procedure by multiplying this time by $x_1(0)$ to obtain the expression of $\langle x_1(t)x_1(0)\rangle$ of eq. (5).

A.6 Evolution of the moments

To meet the Boltzmann equilibrium prediction the random noises f_j in eq. (2) and in eqs. (20)-(21) should verify:

$$\langle f_1(0)f_1(t)\rangle = 2k_B T\gamma \frac{1}{1-\epsilon^2}\delta(t) = \langle f_2(0)f_2(t)\rangle, \tag{25}$$

$$\langle f_1(0)f_2(t)\rangle = -2k_B T\gamma \frac{\epsilon}{1-\epsilon^2}\delta(t). \tag{26}$$

Starting then with the coupled Langevin equation (2), we want to deduce the evolution of the moments of the joint probability in position. To do so we follow the Ito prescription $(\langle f_1(t)x_1(t)\rangle = 0)$ and apply the Ito chain rule on $x_1^2(t)$. Combined with equation (2), and after taking the mean value, we obtain:

$$\gamma\langle x_1 \frac{dx_1}{dt}\rangle = -K_1\langle x_1^2\rangle - \epsilon K_2\langle x_1 x_2\rangle + \epsilon^2\langle f_2^2\rangle + \langle f_1^2\rangle + 2\epsilon\langle f_1 f_2\rangle. \tag{27}$$

Using the auto-correlation values of the f_j's in (25) and (26), we readily obtain:

$$\frac{\gamma}{2}\frac{d\langle x_1^2\rangle}{dt} = -K_1\langle x_1^2\rangle - \epsilon K_2\langle x_1 x_2\rangle + kT. \tag{28}$$

Finally we reproduce the procedure for the other moments and using again dimensionless quantities $(\sigma_{jk} = \langle x_j x_k\rangle\frac{K_{1,i}}{2k_B T})$ we obtain the system to describe the dynamics of the moments given above in eqs. (11), (12) and (13).

A.7 Gaussian behaviour of the coupled particles joint probability distribution

Similarly to the single particle case, we can describe the system through the evolution of its probability density to find the first particle in x_1 and the second in x_2 at time t, $P(x_1, x_2, t)$. The time evolution of the joint Probability $P(x_1, x_2, t)$ is governed by the Fokker-Planck equation:

$$\frac{\partial P}{\partial t} = -\sum_{j=1}^{j=2} \frac{\partial g_j P}{\partial x_j} - \sum_{j,k=1}^{j,k=2} \theta_{jk} \frac{\partial^2 P}{\partial x_j \partial x_k}, \tag{29}$$

where,

$$g_1 = -\frac{1}{\gamma}K_1 x_1 - \frac{\epsilon}{\gamma}K_2 x_2, \tag{30}$$

$$g_2 = -\frac{1}{\gamma}K_2 x_2 - \frac{\epsilon}{\gamma}K_1 x_1, \tag{31}$$

$$\theta_{jj} = \frac{k_B T}{\gamma}, \tag{32}$$

$$\theta_{jk} = \frac{k_B T \epsilon}{\gamma} \text{ for } j \neq k. \tag{33}$$

In order to prove the Gaussian behaviour of the joint Probability, we propose a 2D generalisation of the computation made in ref. [16]. We introduce the 2D Fourier Transform:

$$G(p_1, p_2, t) = \iint_{-\infty}^{+\infty} e^{ip_1 x_1} e^{ip_2 x_2} P(x_1, x_2, t) dx_1 dx_2. \tag{34}$$

We apply this Fourier Transform to Fokker-Plank eq. (29)

$$\frac{\partial G}{\partial t} = -\frac{K_1(p_1 + \epsilon p_2)}{\gamma}\frac{\partial G}{\partial p_1} - \frac{K_2(p_2 + \epsilon p_1)}{\gamma}\frac{\partial G}{\partial p_2} - \frac{k_B T}{\gamma}G[(p_1^2 + p_2^2) + \epsilon p_1 p_2], \tag{35}$$

$$\frac{\partial \ln G}{\partial t} = -\frac{K_1(p_1 + \epsilon p_2)}{\gamma}\frac{\partial \ln G}{\partial p_1} - \frac{K_2(p_2 + \epsilon p_1)}{\gamma}\frac{\partial \ln G}{\partial p_2} - \frac{k_B T}{\gamma}[(p_1^2 + p_2^2) - 2\epsilon p_1 p_2]. \tag{36}$$

On the one hand, the expansion of G generates the moments $\mu_{n,m} = \langle x_1^n x_2^m \rangle$, since $G(p_1, p_2, t) = \sum_{n,m=0}^{+\infty} (ip_1)^n (ip_2)^m \mu_{n,m}(t)/n!m!$. On the other hand the expansion of $\ln(G)$ generates the cumulants $\chi_{n,m}(t)$:

$$\ln G(p_1, p_2, t) = \sum_{n,m=1}^{+\infty} \frac{(ip_1)^n (ip_2)^m}{n!m!} \chi_{n,m}(t). \tag{37}$$

In particular, for example, the two first cumulants in n are the mean and the variance of the first particle position: $\chi_{1,0} = \mu_{1,0} = \langle x_1 \rangle = 0$ and $\chi_{2,0} = \mu_{2,0} - \mu_{1,0}^2 = \langle x_1^2 \rangle - \langle x_1 \rangle^2 = \langle x_1^2 \rangle$. Thus, we identify the power of p_1 and p_2 in eq. (36) and deduce:

$$\gamma \dot{\chi}_{nm} = - (nK_1 + mK_2)\chi_{nm} - \epsilon(mK_1\chi_{n+1,m-1} + nK_2\chi_{n-1,m+1})$$
$$+ 2k_B T(\delta_{n,2}\delta_{m,0} + \delta_{m,2}\delta_{n,0} + \epsilon\delta_{m,1}\delta_{n,1}). \tag{38}$$

For $(n, m) = (2, 0)$ (that corresponds to σ_{11}), $(n, m) = (0, 2)$ (σ_{22}), and $(n, m) = (1, 1)$ (σ_{12}), we recover the evolution equations eq. (11)-(13). But in addition, eq. (38) for $(n + m) > 2$ entails that an initially Gaussian distribution remains Gaussian at all times. Indeed we easily deduce that if $\chi_{n,m}(0) = 0$ for all $(n + m) > 2$ in the equilibrium state, we have $\chi_{n,m}(t) = 0$ for all time for all $(n + m) > 2$.

A.8   Coupled ESE enforcing independence

Requesting particle independence at all times demands that $\sigma_{12} = 0$. We can then simplify the evolution eqs. (11)-(13) into:

$$\Gamma \frac{d\sigma_{11}}{ds} = -2k_1\sigma_{11} + 1, \tag{39}$$

$$\Gamma \frac{d\sigma_{22}}{ds} = -2k_2\sigma_{22} + 1, \tag{40}$$

$$1 = k_2\sigma_{22} + k_1\sigma_{11}. \tag{41}$$

We straightforwardly deduce how the second particle variance is linked to the first and how the two stiffness profiles are related,

$$\sigma_{22}(s) = -\sigma_{11}(s) + \frac{1}{2} + \frac{1}{k_{2i}}, \tag{42}$$

$$k_2(s) = \frac{2k_{2i}(1 - k_1(s)\sigma_{11}(s))}{k_{2i} - 2k_{2i}\sigma_{11}(s) + 2}. \tag{43}$$

Moreover, we observe that eq. (39) that describes the σ_{11} evolution is the same as in the single particle case. Thus if we impose the same ESE profile on $k_1(s)$, the equilibrium requirements on the 1st particle will be met. The corresponding $k_2(s)$ can be deduced from eq. (43). We finally obtain for the coupled particles ESE protocol:

$$k_1(s) = 1 + (k_{1f} - 1)(3 - 2s)s^2 - \frac{3\Gamma(k_{1f} - 1)(s - 1)s}{1 + (k_{1f} - 1)(3 - 2s)s^2}, \tag{44}$$

$$k_2(s) = 1 + (k_{1f} - 1)(3 - 2s)s^2$$
$$+ \frac{3\Gamma(k_{1f} - 1)(s - 1)s}{1 + (k_{1f} - 1)(3 - 2s)s^2} \frac{k_{2i}}{1 + (1 + k_{2i})(k_{1f} - 1)(3 - 2s)s^2}. \tag{45}$$

A.9   Symmetric coupled ESE solution

We explored a new family of ESE solutions adapted to the coupled system by proposing the *coupled ESE* enforcing independence between the particles, at the expense of having the evolution of particle 2 enslaved to that of particle 1, and thereby not a priori controlled. This has the consequence that the two particles cannot be treated symmetrically. It is thus interesting to look for another solution to the coupled problem: an ESE protocol that jointly drives the two potentials and treats the two particles in a symmetric fashion. Such a protocol will introduce cross-correlation between particles contrary to the *coupled ESE* enforcing independence.

Now that we require for all time $K_1(t) = K_2(t) = K(t)$ (and so $\sigma_{11}(t) = \sigma_{22}(t)$), from evolution equations arise two modes $u = \sigma_{11} + \sigma_{12}$ and $v = \sigma_{11} - \sigma_{12}$ that satisfy the following decoupled system:

$$\Gamma \frac{du}{ds} = -2k(s)(1+\epsilon)u(s) + (1+\epsilon), \tag{46}$$

$$\Gamma \frac{dv}{ds} = -2k(s)(1-\epsilon)v(s) + (1-\epsilon). \tag{47}$$

The modes evolve following the same form of equations with 2 different time scales $\tau_u < \tau_v$ that correspond to the τ_- and τ_+ appearing into the correlation functions for the symmetric case. Indeed one may notice that $u = \sigma_{11} + \sigma_{12} = 2\langle x_M^2 \rangle$ and $v = \sigma_{11} - \sigma_{12} = 2\langle x_\mu^2 \rangle$. We naturally recover the modes corresponding to the barycentre and the fictitious particle movement, with the barycentre moving faster because it does not require the displacement of the fluid between the particles to move.

The strategy to exhibit an ESE protocol from eqs. (46)-(47) is the following: first we propose a fifth order polynomial form of $v(s)$ with one degree of freedom (called parameter p) satisfying initial and final conditions of equilibrium. Secondly, find the expression of $u(s)$ as a function of $v(s, p)$:

$$u(s) = \frac{1}{I(s)} \left(1 + \frac{2(1+\epsilon)}{\Gamma} \right) \int_0^s I(y)dy, \tag{48}$$

with

$$I(y) = \exp \left\{ \frac{2(1+\epsilon)}{\Gamma} \int_0^y k(x)dx \right\} = \exp \left\{ \frac{1+\epsilon}{1-\epsilon} \int_0^y \frac{(1-\dot{v}(x))}{v(x)} dx \right\}. \tag{49}$$

Finally, tune the parameter p of the ansatz of $v(s)$ to satisfy boundary conditions for $u(s)$ from eq. (48). A simple procedure of dichotomy that iterates on the value of the p parameter does the job. Knowing the expression of $u(s)$ and $v(s)$, the stiffness profile can be easily deduced from eq. (46).

Fig. 9 plots an example of *symmetric coupled ESE protocol* obtained with this procedure. It is important to point out that this protocol that guides jointly the two particles of a coupled system depends on the coupling intensity (ϵ). This property makes it hard to implement experimentally.
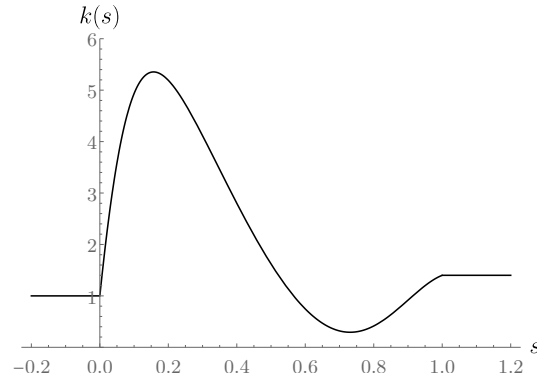
Figure 9: Stiffness profile for the symmetric coupled ESE treating particles distant by $d = 0.7\,\mu$m (coupling constant $\epsilon = 0.5$). Both potentials are controlled by the same protocol that leads the particles from K_i to $K_f = k_f \times K_i$ in the desired time t_f. The parameters of the ESE plotted here are: $t_f = 3\,$ms, $K_i = 2.5 \times 10^{-6}\,$N/m, $k_f = 1.4$ and $\Gamma = 2.5$

References

[1] D. S. Lobser, A. E. S. Barentine, E. A. Cornell and H. J. Lewandowski, *Observation of a persistent non-equilibrium state in cold atoms*, Nature Physics **11**(12), 1009 (2015), doi:10.1038/nphys3491.

[2] D. Guéry-Odelin and E. Trizac, *Boltzmann avenged*, Nature Physics **11**(12), 988 (2015), doi:10.1038/nphys3522.

[3] D. Guéry-Odelin, J. G. Muga, M. J. Ruiz-Montero and E. Trizac, *Nonequilibrium solutions of the boltzmann equation under the action of an external force*, Phys. Rev. Lett. **112**, 180602 (2014), doi:10.1103/PhysRevLett.112.180602.

[4] D. Guéry-Odelin, A. Ruschhaupt, A. Kiely, E. Torrontegui, S. Martínez-Garaot and J. G. Muga, *Shortcuts to adiabaticity: Concepts, methods, and applications*, Rev. Mod. Phys. **91**, 045001 (2019), doi:10.1103/RevModPhys.91.045001.

[5] G. Li, H. T. Quan and Z. C. Tu, *Shortcuts to isothermality and nonequilibrium work relations*, Physical Review E **96**(1), 012144 (2017), doi:10.1103/PhysRevE.96.012144.

[6] I. A. Martínez, A. Petrosyan, D. Guéry-Odelin, E. Trizac and S. Ciliberto, *Engineered swift equilibration of a Brownian particle*, Nature Physics **12**(9), 843 (2016), doi:10.1038/nphys3758.

[7] A. Bérut, A. Petrosyan and S. Ciliberto, *Energy flow between two hydrodynamically coupled particles kept at different effective temperatures*, Europhysics Lett. **107**(6), 60004 (2014), doi:10.1209/0295-5075/107/60004.

[8] A. Bérut, A. Imparato, A. Petrosyan and S. Ciliberto, *Theoretical description of effective heat transfer between two viscously coupled beads*, Physical Review E **94**(5), 052148 (2016), doi:10.1103/PhysRevE.94.052148.

[9] J.-C. Meiners and S. R. Quake, *Direct Measurement of Hydrodynamic Cross Correlations between Two Particles in an External Potential*, Physical Review Letters **82**(10), 2211 (1999), doi:10.1103/PhysRevLett.82.2211.

[10] S. E. M.Doi, *The Theory of Polymer Dynamics*, International Series of Monographs on Physics (1988).

[11] S. Herrera-Velarde, E. C. Euán-Díaz, F. Córdoba-Valdés and R. Castañeda-Priego, *Hydrodynamic correlations in three-particle colloidal systems in harmonic traps*, Journal of Physics: Condensed Matter **25**(32), 325102 (2013), doi:10.1088/0953-8984/25/32/325102.

[12] J. A. C. Albay, P.-Y. Lai and Y. Jun, *Realization of finite-rate isothermal compression and expansion using optical feedback trap*, Applied Physics Letters **116**(10), 103706 (2020), doi:10.1063/1.5143602.

[13] M. Chupeau, B. Besga, D. Guéry-Odelin, E. Trizac, A. Petrosyan and S. Ciliberto, *Thermal bath engineering for swift equilibration*, Physical Review E **98**(1), 010104 (2018), doi:10.1103/PhysRevE.98.010104.

[14] A. Bérut, *Fluctuations and Interactions of Brownian particles in multiple Optical Traps*, PhD Thesis, Ecole Normale Supérieure de Lyon - ENS LYON, `https://tel.archives-ouvertes.fr/tel-01192759` (2015).

[15] J. Leach, H. Mushfique, S. Keen, R. Di Leonardo, G. Ruocco, J. M. Cooper and M. J. Padgett, *Comparison of faxén's correction for a microsphere translating or rotating near a surface*, Phys. Rev. E **79**, 026301 (2009), doi:10.1103/PhysRevE.79.026301.

[16] C. A. Plata, D. Guéry-Odelin, E. Trizac and A. Prados, *Finite-time adiabatic processes: Derivation and speed limit*, Phys. Rev. E **101**, 032129 (2020), doi:10.1103/PhysRevE.101.032129.